AD-A095 886   CAMBRIDGE HYDRODYNAMICS INC MA   F/G 12/1
                APPLICATIONS OF NUMERICAL CONFORMAL MAPPING.(U)
                JUL 80 D I MEIRON, S A ORSZAG, M ISRAELI   N00014-80-C-0127
UNCLASSIFIED   CHI-34   NL

END
DATE
FILMED
4-84
DTIC

CAMBRIDGE HYDRODYNAMICS REPORT NO. 34

APPLICATIONS OF NUMERICAL CONFORMAL MAPPING

DANIEL I. MEIRON, STEVEN A. ORSZAG,

AND MOSHE ISRAELI

(14) CHI-34

REPORT DOCUMENTATION PAGE	READ INSTRUCTIONS BEFORE COMPLETING FORM

1. REPORT NUMBER	2. GOVT ACCESSION NO. AD-AO95886	3. RECIPIENT'S CATALOG NUMBER

4. TITLE (and Subtitle)	5. TYPE OF REPORT & PERIOD COVERED
Cambridge Hydrodynamics Report No. 34 (9) Applications of Numerical Conformal Mapping.	Interim Technical Report.
	6. PERFORMING ORG. REPORT NUMBER CHI Report No. 34

7. AUTHOR(s)	8. CONTRACT OR GRANT NUMBER(s)
Daniel I. Meiron, Steven A. Orszag (15) and Moshe Israeli	N00014-80-C-0127

9. PERFORMING ORGANIZATION NAME AND ADDRESS	10. PROGRAM ELEMENT, PROJECT, TASK AREA & WORK UNIT NUMBERS
Cambridge Hydrodynamics, Inc. P.O. Box 249, MIT Station Cambridge, MA 02139	

11. CONTROLLING OFFICE NAME AND ADDRESS	12. REPORT DATE
David W. Taylor Naval Ship Research and Development Center Bethesda, MD 20084	Jul 80
	13. NUMBER OF PAGES 35

14. MONITORING AGENCY NAME & ADDRESS(if different from Controlling Office)	15. SECURITY CLASS. (of this report)
Office of Naval Research 800 N. Quincy Street Arlington, VA 22217	Unclassified
	15a. DECLASSIFICATION/DOWNGRADING SCHEDULE

16. DISTRIBUTION STATEMENT (of this Report)

APPROVED FOR PUBLIC RELEASE; DISTRIBUTION UNLIMITED

17. DISTRIBUTION STATEMENT (of the abstract entered in Block 20, if different from Report)

18. SUPPLEMENTARY NOTES

This work was sponsored by the Naval Sea Systems Command General Hydromechanics Research (GHR) Program administered by the David W. Taylor Naval Ship R&D Center Bethesda, Md 20084 (Code 1505)

19. KEY WORDS (Continue on reverse side if necessary and identify by block number)

Conformal mapping
Water waves
Rayleigh-Taylor instability
Potential theory

Free-surface flows

20. ABSTRACT (Continue on reverse side if necessary and identify by block number)

The application of conformal mapping methods to the solution of free-surface flow problems is considered. Methods of numerical conformal mapping based on Fourier series are extended to handle efficiently problems with time-dependent boundaries. They are shown to be practicable only for moderately distorted geometries. Extensions of the Menikoff-Zemach method to breaking geometries are presented. This method works well at large distortions.

DD FORM 1473 EDITION OF 1 NOV 65 IS OBSOLETE
1 JAN 73

393391

INSTRUCTIONS FOR PREPARATION OF REPORT DOCUMENTATION PAGE

RESPONSIBILITY. The controlling DoD office will be responsible for completion of the Report Documentation Page, DD Form 1473, in all technical reports prepared by or for DoD organizations.

CLASSIFICATION. Since this Report Documentation Page, DD Form 1473, is used in preparing announcements, bibliographies, and data banks, it should be unclassified if possible. If a classification is required, identify the classified items on the page by the appropriate symbol.

COMPLETION GUIDE

General. Make Blocks 1, 4, 5, 6, 7, 11, 13, 15, and 16 agree with the corresponding information on the report cover. Leave Blocks 2 and 3 blank.

Block 1. Report Number. Enter the unique alphanumeric report number shown on the cover.

Block 2. Government Accession No. Leave Blank. This space is for use by the Defense Documentation Center.

Block 3. Recipient's Catalog Number. Leave blank. This space is for the use of the report recipient to assist in future retrieval of the document.

Block 4. Title and Subtitle. Enter the title in all capital letters exactly as it appears on the publication. Titles should be unclassified whenever possible. Write out the English equivalent for Greek letters and mathematical symbols in the title (see "Abstracting Scientific and Technical Reports of Defense-sponsored RDT/E," AD-667 000). If the report has a subtitle, this subtitle should follow the main title, be separated by a comma or semicolon if appropriate, and be initially capitalized. If a publication has a title in a foreign language, translate the title into English and follow the English translation with the title in the original language. Make every effort to simplify the title before publication.

Block 5. Type of Report and Period Covered. Indicate here whether report is interim, final, etc., and, if applicable, inclusive dates of period covered, such as the life of a contract covered in a final contractor report.

Block 6. Performing Organization Report Number. Only numbers other than the official report number shown in Block 1, such as series numbers for in-house reports or a contractor/grantee number assigned by him, will be placed in this space. If no such numbers are used, leave this space blank.

Block 7. Author(s). Include corresponding information from the report cover. Give the name(s) of the author(s) in conventional order (for example, John R. Doe or, if author prefers, J. Robert Doe). In addition, list the affiliation of an author if it differs from that of the performing organization.

Block 8. Contract or Grant Number(s). For a contractor or grantee report, enter the complete contract or grant number(s) under which the work reported was accomplished. Leave blank in in-house reports.

Block 9. Performing Organization Name and Address. For in-house reports enter the name and address, including office symbol, of the performing activity. For contractor or grantee reports enter the name and address of the contractor or grantee who prepared the report and identify the appropriate corporate division, school, laboratory, etc., of the author. List city, state, and ZIP Code.

Block 10. Program Element, Project, Task Area, and Work Unit Numbers. Enter here the number code from the applicable Department of Defense form, such as the DD Form 1498, "Research and Technology Work Unit Summary" or the DD Form 1634, "Research and Development Planning Summary," which identifies the program element, project, task area, and work unit or equivalent under which the work was authorized.

Block 11. Controlling Office Name and Address. Enter the full, official name and address, including office symbol, of the controlling office. (Equates to funding/sponsoring agency. For definition see DoD Directive 5200.20, "Distribution Statements on Technical Documents.")

Block 12. Report Date. Enter here the day, month, and year or month and year as shown on the cover.

Block 13. Number of Pages. Enter the total number of pages.

Block 14. Monitoring Agency Name and Address (if different from Controlling Office). For use when the controlling or funding office does not directly administer a project, contract, or grant, but delegates the administrative responsibility to another organization.

Blocks 15 & 15a. Security Classification of the Report: Declassification/Downgrading Schedule of the Report. Enter in 15 the highest classification of the report. If appropriate, enter in 15a the declassification/downgrading schedule of the report, using the abbreviations for declassification/downgrading schedules listed in paragraph 4-207 of DoD 5200.1-R.

Block 16. Distribution Statement of the Report. Insert here the applicable distribution statement of the report from DoD Directive 5200.20, "Distribution Statements on Technical Documents."

Block 17. Distribution Statement (of the abstract entered in Block 20, if different from the distribution statement of the report). Insert here the applicable distribution statement of the abstract from DoD Directive 5200.20, "Distribution Statements on Technical Documents."

Block 18. Supplementary Notes. Enter information not included elsewhere but useful, such as: Prepared in cooperation with . . . Translation of (or by) . . . Presented at conference of . . . To be published in . . .

Block 19. Key Words. Select terms or short phrases that identify the principal subjects covered in the report, and are sufficiently specific and precise to be used as index entries for cataloging, conforming to standard terminology. The DoD "Thesaurus of Engineering and Scientific Terms" (TEST), AD-672 000, can be helpful.

Block 20. Abstract. The abstract should be a brief (not to exceed 200 words) factual summary of the most significant information contained in the report. If possible, the abstract of a classified report should be unclassified and the abstract to an unclassified report should consist of publicly- releasable information. If the report contains a significant bibliography or literature survey, mention it here. For information on preparing abstracts see "Abstracting Scientific and Technical Reports of Defense-Sponsored RDT&E," AD-667 000.

Abstract

The application of conformal mapping methods to
the solution of free-surface flow problems is considered.
Methods of numerical conformal mapping based on Fourier
series are extended to handle efficiently problems with
time-dependent boundaries. They are shown to be
practicable only for moderately distorted geometries.
Extensions of the Menikoff-Zemach method to 'breaking'
geometries are presented. These latter methods are
robust at quite large distortions, but degrade
prematurely in time-dependent problems at amplitudes
smaller than achieved by our recent vortex methods.

1. INTRODUCTION

In this paper, we investigate the application of conformal mapping to the solution of time-dependent potential flow problems, such as Rayleigh-Taylor instability and water waves. We begin by formulating the water wave problem. For two-dimensional, incompressible, irrotational, free-surface flow, the velocity is expressible as $\underset{\sim}{v} = \underset{\sim}{\nabla}\phi$, where the potential ϕ satisfies Laplace's equation $\nabla^2\phi = 0$ in the region $y < \eta(x,t)$ beneath the free surface $y = \eta(x,t)$. Since the free surface moves with the fluid,

$$\frac{Dx}{Dt} = \phi_x, \quad \frac{Dy}{Dt} = \phi_y, \quad (y = \eta(x,t)), \qquad (1.1)$$

where D/Dt is a Lagrangian derivative. Bernoulli's law is satisfied throughout the fluid so that

$$\frac{D\phi}{Dt} = -\eta(x,t) + \frac{1}{2}v^2 - p_s \qquad (1.2)$$

at the free surface $y = \eta(x,t)$, where the gravitational acceleration is normalized to unity and p_s is the applied surface pressure. It is assumed below that the free surface is periodic in x with wavelength 2π.

In order to march forward in time, it is necessary to know $\nabla\phi$ at the free surface. If ϕ is known then its tangential derivative $\partial\phi/\partial s$ is computable but its normal derivative $\partial\phi/\partial n$ must be found by solving Laplace's equation. Green's third formula expresses $\partial\phi/\partial n$ in terms of ϕ :

$$\int_{\partial D} \frac{\partial}{\partial n} \, \ln|\underset{\sim}{p}-\underset{\sim}{q}|\phi(q)\,d\underset{\sim}{q} - \int_{\partial D} \ln|\underset{\sim}{p}-\underset{\sim}{q}| \, \frac{\partial\phi}{\partial n}(q)\,d\underset{\sim}{q} = 2\pi\phi(\underset{\sim}{p}).$$

(1.3)

Here $\underset{\sim}{p},\underset{\sim}{q}$ are vectors lying on the boundary ∂D of the region D. Eq. (1.3) is a linear integral equation of the first kind for the unknown function $\partial\phi/\partial n$. Once $\partial\phi/\partial n$ has been calculated, Eq. (1.1) and (1.2) may be used to update the free surface and potential.

Numerical solution of (1.3) for $\partial\phi/\partial n$ involves the approximation of its logarithmic kernel by a finite matrix. If the continuous boundary is approximated by N discrete points, the operation count for the solution of the resulting linear system is $O(N^3)$ since the matrix is full. In addition, storage of the matrix requires $O(N^2)$ memory locations. For large N the computational costs are prohibitive.

Our work is motivated by the desire to develop algorithms with decreased operation counts and storage requirements for solving free surface potential flow problems. We have recently proposed a new vortex method[1,2] to solve these problems with $O(N)$ memory and $O(N^2)$ operations per time step. In the present paper, two conformal mapping methods are studied. Both require only $O(N)$ memory. The methods discussed in Sec. 2 require only $O(N \log_2 N)$ operations per time step but are effectively limited to modest surface deformations. In Sec. 3, modifications of the Menikoff-Zemach method[10] that require $O(N^2)$ operations per time step are introduced. Larger surface deformations can be handled accurately by these latter methods.

2. CONFORMAL MAPPING USING FOURIER SERIES

In this Section, numerical methods are developed to compute the conformal map $z(\zeta)$ of the unit disk $|\zeta| \leq 1$ onto a simply connected finite region D in the complex-z plane. A map of the unit disk onto a semi-infinite periodic region $R: w = x+iy$, $0 \leq x \leq 2\pi$, $y < \eta(x)$, is given by

$$w = i \ln \, z(\zeta) \tag{2.1}$$

where $z(\zeta)$ is a map of the unit disk onto the interior of the region with boundary

$$z = \exp[-ix + \eta(x)].$$

This sequence of conformal maps is depicted in Fig. 1.

Before proceeding to the discussion of methods to compute the conformal map $z(\zeta)$, we note that knowledge of $z(\zeta)$ allows efficient solution of potential problems in the region R. If $\phi(w)$ is harmonic in R then $\phi(i \ln z(\zeta))$ is harmonic in the unit disk. Therefore, the Dirichlet problem can be solved by Poisson's formula. Also, since conformal maps are angle preserving, the normal derivative $\partial\phi/\partial n$ of ϕ on the boundary $\setminus$ R is related to the radial derivative $\partial\phi/\partial\rho$ of ϕ on $|\zeta| = \rho = 1$:

$$\left.\frac{\partial\phi}{\partial n}\right|_{y=\eta(x)} = \left.\frac{\partial\phi}{\partial\rho}\right|_{\rho=1} \left.\left|\frac{z(\zeta)}{\frac{dz}{d\zeta}}\right|\right._{\rho=1} \tag{2.2}$$

The derivative $dz/d\zeta$ can not vanish for $|\zeta| \leq 1$ if $z(\zeta)$ is single-valued.

Let us begin by characterizing the analytic character of $z(\zeta)$ in terms of Fourier series. The boundary values $z(e^{i\alpha})$ of the conformal map $z(\zeta)$ are a periodic function of the angle α on the unit disk so

$$z(e^{i\alpha}) = \sum_{k=-\infty}^{\infty} A_k \, e^{ik\alpha} \qquad (2.3)$$

The condition that $z(\zeta)$ be analytic is

$$A_k = 0, \quad k < 0 \qquad (2.4)$$

and, in this case, $z(\zeta)$ is given explicitly by

$$z(\zeta) = \sum_{k=0}^{\infty} A_k \, \zeta^k \qquad (2.5)$$

In other words, an analytic transformation of the unit disk onto a region D is equivalent to a parametrization of ∂D in terms of α such that the Fourier representation of ∂D has only positive frequency components.

Now we consider a discrete approximation to the conformal map. Consider the equally spaced discrete points $\alpha_j = \sigma j$ ($j = 0, \ldots N-1$), where $\sigma = 2\pi/N$, and the associated points z_j on ∂D. Then z_j can be represented as the finite Fourier series

$$z_j = z(e^{i\sigma j}) = \sum_{-\frac{N}{2}\le k<\frac{N}{2}} a_k \, e^{ik\sigma j} \quad (0\le j<N). \qquad (2.6)$$

It may easily be shown that

$$a_k = A_k + \sum_{p \neq 0} A_{k+pN} \qquad (2.7)$$

One way to determine an approximation to the conformal map $z(\zeta)$ is to require that $a_k = 0$ for $k < 0$. Indeed, if N is large enough that A_k is negligible for $k > N$, then a_k is negligibly small for $k < 0$. This idea may be used to obtain iterative methods[4-8] based on the fast Fourier transform (FFT) to compute the approximate conformal map. These methods typically require $O(N \log_2 N)$ operations per iteration. We note that for any a_k satisfying $a_k = 0$ for $k < 0$, the resulting conformal map

$$\hat{z}(\zeta) = \sum_{0 \leq k < N/2} a_k \zeta^k \qquad (2.8)$$

satisfies $\hat{z}(e^{i\sigma j}) = z_j$. Thus, the map z transforms the N equally spaced points $e^{i\sigma j}$ into points z_j lying on ∂D.

As an alternative to these iterative methods, we have obtained a differential equation which relates the time rate of change of the conformal map to the time rate of change of a moving boundary. This differential equation is well suited to the solution of free surface flow problems where the solution of the potential problem determines the time rate of change of the free surface.

Let the boundary be represented for all time t by the equation

$$F(z(\alpha,t),\ \overline{z}(\alpha,t),t) = 0. \tag{2.9}$$

Differentiation of (2.8) with respect to t yields

$$\frac{\partial F}{\partial t} + \frac{\partial F}{\partial z}\ \frac{\partial z}{\partial t} + \frac{\partial F}{\partial \overline{z}}\ \frac{\partial \overline{z}}{\partial t} = 0, \tag{2.10}$$

and differentiation with respect to the angle α (see Fig. 1) gives

$$\frac{\partial F}{\partial z}\ \frac{\partial z}{\partial \alpha} + \frac{\partial F}{\partial \overline{z}}\ \frac{\partial \overline{z}}{\partial \alpha} = 0. \tag{2.11}$$

The relation

$$\mathrm{Im}\left(\frac{\frac{\partial z}{\partial t}}{\frac{\partial z}{\partial \alpha}}\right) = \frac{i}{2}\ \frac{\frac{\partial F}{\partial t}}{\frac{\partial F}{\partial z}\ \frac{\partial z}{\partial \alpha}} \tag{2.12}$$

is obtained by substituting (2.11) into (2.10). This equation only provides the imaginary part of $\frac{\partial z}{\partial t}\Big/\frac{\partial z}{\partial \alpha}$. The real part of $\frac{\partial z}{\partial t}\Big/\frac{\partial z}{\partial \alpha}$ is determined by requiring that it be analytic in the domain described by (2.9).

The right hand side of (2.12) is real and can be represented by a conjugate symmetric Fourier series:

$$\frac{i}{2} \frac{\frac{\partial F}{\partial t}}{\frac{\partial F}{\partial z} \frac{\partial z}{\partial \alpha}} = \text{Re} \left[\sum_{m=0}^{\frac{1}{2}N-1} b_m \exp(im\alpha) \right]$$

Therefore, analytic continuation of (2.12) gives

$$\frac{\partial z}{\partial t} = i \frac{\partial z}{\partial \alpha} \sum_{m=0}^{\frac{1}{2}N-1} b_m \exp(im\alpha) \qquad (2.13)$$

where

$$\frac{\partial z}{\partial \alpha} = \sum_{k=0}^{\frac{1}{2}N-1} (ik) a_k \exp ik\alpha) \qquad (2.14)$$

The right hand side of Eq. (2.12) is directly related to the normal velocity of the moving boundary. In Cartesian coordinates

$$F(z,\bar{z},t) = y - \eta(x,t) \qquad (2.15)$$

so

$$\frac{\partial F}{\partial t} = - \frac{\partial \eta}{\partial t} \qquad (2.16)$$

Also,

$$\frac{\partial F}{\partial z} \frac{\partial z}{\partial \alpha} = \frac{1}{2} \left(\frac{\partial F}{\partial x} - i \frac{\partial F}{\partial y}\right) \left(\frac{\partial x}{\partial \alpha} + i \frac{\partial y}{\partial \alpha}\right) \qquad (2.17)$$

Substitution of (2.16) and (2.17) into (2.12) gives

$$\text{Im}\left(\dfrac{\frac{\partial z}{\partial t}}{\frac{\partial z}{\partial \alpha}}\right) = \dfrac{\frac{\partial \eta}{\partial t}}{\frac{\partial x}{\partial \alpha} + \frac{\partial \eta}{\partial x}\frac{\partial y}{\partial \alpha}} \tag{2.18}$$

The free surface condition (1.1) can be written as

$$\frac{\partial \eta}{\partial t} = \frac{\partial \phi}{\partial y} - \frac{\partial \eta}{\partial x}\frac{\partial \phi}{\partial x} \tag{2.19}$$

Using the decomposition of $\partial\phi/\partial x$ and $\partial\phi/\partial y$ into tangential and normal components

$$\frac{\partial \phi}{\partial y} = \left(\frac{\partial y}{\partial s}\frac{\partial \phi}{\partial s} - \frac{\partial x}{\partial s}\frac{\partial \phi}{\partial n}\right)$$

$$\frac{\partial \phi}{\partial x} = \left(\frac{\partial x}{\partial s}\frac{\partial \phi}{\partial s} + \frac{\partial y}{\partial s}\frac{\partial \phi}{\partial n}\right) \tag{2.20}$$

in (2.18) gives the final result in terms of the polar coordinates ρ and α :

$$\text{Im}\left[\dfrac{\frac{\partial z}{\partial t}}{\frac{\partial z}{\partial \alpha}}\right] = - \left.\frac{\partial \phi}{\partial \rho}\right|_{\rho=1} \left|\dfrac{z}{\frac{\partial z}{\partial \alpha}}\right|^2 \tag{2.21}$$

An analogous result was obtained using perturbation methods by Kantorovich and Krylov.[8]

-10-

Eq. (2.21) describes the motion of points following the conformal map of the free surface rather than the Lagrangian or Eulerian paths. Bernoulli's equation (1.2) must also be modified to take this fact into account:

$$\frac{D\phi}{Dt} = - \ln|z| - \frac{1}{2}\left[\left(\frac{\partial\phi}{\partial\rho}\right)^2 + \left(\frac{\partial\phi}{\partial\alpha}\right)^2 \right] \left| \frac{z}{\frac{\partial z}{\partial\alpha}} \right|^2 \qquad (2.22)$$

$$+ \frac{\partial\phi}{\partial x} \frac{Dx}{Dt} + \frac{\partial\phi}{\partial y} \frac{Dy}{Dt}$$

Once the conformal map (2.4) from the unit circle is known, the solution of the Dirichlet problem may be given in terms of a Fourier series

$$\phi(\rho e^{i\alpha}) = \sum_{n=0}^{\frac{1}{2}N-1} [g_n \rho^n \cos n\alpha + h_n \rho^n \sin n\alpha] \qquad (2.23)$$

On the unit circle ($\rho = 1$) the tangential and normal derivatives are given by

$$\frac{\partial\phi}{\partial\alpha} = \sum_{n=0}^{\frac{1}{2}N-1} [-ng_n \sin n\alpha + n h_n \cos n\alpha] \qquad (2.24)$$

$$\frac{\partial\phi}{\partial\rho} = \sum_{n=0}^{\frac{1}{2}N-1} [ng_n \cos n\alpha + nh_n \sin n\alpha], \qquad (2.25)$$

which are computable using FFT's in $O(N \log_2 N)$ operations.

-11-

Now let us summarize the steps involved in marching
from time t to $t + \Delta t$ by this method. At time t,
the points $\{z_j\}$ and potentials $\{\phi_j\}$ are assumed known.
First, the coefficients g_n, h_n in (2.23) are obtained
from $\{\phi_j\}$ using an FFT. Next, $\vec{\nabla}\phi$ is computed on the
boundary using (2.24) and (2.25). Then ϕ_j is
updated by (2.22) and z_j is updated by (2.21).
The total operation count is $0(N \log_2 N)$. Note that the
conformal map is uniquely defined by (2.21) and the
supplementary conditions $a_0 = 0$, $\text{Im}(a_1) = 0$.

As a test of this time dependent mapping method,
we study the propagation of Stokes' permanent water waves.
In a frame of reference moving with the wave speed, the
numerically calculated profiles should be steady. The
initial conditions for the calculation are obtained using
Padé approximants of perturbation expansions of the Stokes
waves[11]. The time-dependent equations (2.21), (2.22)
are solved by a fourth-order Adams-Moulton predictor
corrector scheme. As with other simulations of propagating
nonlinear water waves,[2,9] an instability of the free
surface quickly develops unless damping is applied. To
remove this instability, we periodically apply a five-
point smoothing operator[9].

For a Stokes wave with peak-to-trough amplitude 80%
of the maximum allowed by theory, we choose the time step
to be $2\pi/400$ with wavelength 2π and apply smoothing

every tenth step. The resulting wave profile is plotted
in Fig. 2. The dots indicate the position of the points
z_j used to calculate the conformal map of the wave.
The solid line is the wave profile computed by Padé approximants[11],
translated by an amount equal to the nonlinear phase speed
multiplied by the time. The computation time for one
evaluation of the time derivatives of the map and potential
is 3ms on the CRAY-1 computer using $N = 64$ points. The
total computation time for the motion of the wave through
one period is about 1s.

The conformal mapping method described here works
well provided the region is not highly distorted. As
the region of interest becomes more distorted the points
corresponding to the conformal map tend to crowd[3,10].
For example, consider the conformal mapping from the unit
disk to the region lying below $y = A \cos kx$. The number
of terms N that must be retained in the Fourier expansion
(2.4) to obtain a good representation of this map satisfies
$\ln N \sim \gamma kA$ as $kA \to \infty$,[3] where $\gamma = \dfrac{\pi}{2} \displaystyle\int_0^\pi \dfrac{\sin x}{x}\, dx \simeq 2.909$,
showing the difficulty of mapping from the unit disk to a
deformed region.

When N is large, almost all of the equally spaced
points $e^{i\sigma_j}$ on the unit circle are mapped into points
z_j that are crowded into small intervals on the boundary
of the domain D. Dubiner[3] has recently made a detailed
analysis of this problem and has shown that the crowding
occurs whenever the region being mapped has a 'narrow'

section. This effect occurs in high amplitude Rayleigh-Taylor instability and in breaking waves. The FFT method is not effective in dealing with these highly distorted geometries.

When the domain D is highly deformed, the iterative methods[4-8] and our differential equation method do give a conformal map of the unit disk onto a domain that passes through the desired points z_j of ∂D. However, unless N is unreasonably large, the conformal map so obtained will have large deviations from ∂D between the points z_j. Indeed, (2.8) gives an accurate conformal map of ∂D only if a_k decreases rapidly as k increases to $\frac{1}{2}N$.

One possible approach to the crowding problem is to use a sequence of mappings of the disk onto successively more highly deformed regions. Such iterated mappings are still under study. For such methods, one result seems assured, namely that the operation counts must degrade from $0(N \log_2 N)$ to $0(N^2)$ or worse. In this case, these Fourier series methods are probably inferior to the methods to be described in Sec. 3.

3.   APPLICATION OF THE MENIKOFF-ZEMACH METHOD

The Fourier series methods for mapping the unit disk onto D can not accurately handle highly distorted domains as the crowding phenomenon causes a severe loss of resolution

in some part of the physical boundary. This difficulty

may be overcome by mapping D onto the unit disk with

a regular distribution of points on ∂D. The crowding

then occurs on the boundary of the unit disk. Even

with a highly nonuniform distribution of points on the

unit circle, the potential problem in the unit disk is

still readily solved by Poisson's formula.

Recently, Menikoff and Zemach[10] have developed a

new nonlinear integral equation for conformal mapping

of the region R above $y = \eta(x)$ onto the periodic

semi-infinite strip $S: 0 \le u < 2\pi$, $0 \le v < \infty$. Their method

requires relatively few points to achieve accurate

results for distorted domains.

A simple extension of Menikoff and Zemach's equation

which is valid for general periodic interfaces is

derived here and is used to investigate the crowding

phenomenon for multivalued (or 'breaking wave') interfaces.

A time dependent version of the equation is also developed.

This approach reduces to the integration of N nonlinear

differential equations.

The Menikoff-Zemach equations, generalized to handle

conformal maps of a domain with boundary curve parametrized

as $x = x(e)$, $y = y(e)$, are

$$y(e) = y_\infty + 2 \int_0^{2\pi} \ln \frac{\sin \frac{1}{2}(u(e)-u(e'))}{\sin \frac{1}{2}(e-e')} \frac{dx}{de'}(e') \frac{de'}{2\pi}$$

$$+ \int_0^{2\pi} \cot \left(\frac{e-e'}{2}\right) [(x(e')-e') - (x(e)-e)] \frac{de'}{2\pi} \qquad (3.1a)$$

$$u(e) = x(e) - x_\infty + 2 \int_0^{2\pi} \ln \left| \frac{\sin \frac{1}{2}(u(e)-u(e'))}{\sin \frac{1}{2}(e-e')} \right| \frac{dy}{de'} \frac{de'}{2\pi}$$

$$+ \int_0^{2\pi} \cot \left(\frac{e-e'}{2}\right) [y(e')-y(e)] \frac{de'}{2\pi} . \qquad (3.1b)$$

Here e is chosen so that $x(0) = 0$, $x(2\pi) = 2\pi$, $u(e)$ is defined so $(x(e),y(e))$ is mapped into $(u(e),0)$, and y_∞, x_∞ are determined by the condition that $u(0) = 0$. Note that (3.1a) and (3.1b) are equivalent; either one can be used to determine $u(e)$. Once $u(e)$ is found by solution of (3.1), the conformal map is determined.

Eqs. (3.1) are derived from the pair of Hilbert transforms:

$$Re[G(u,0)] = Re(G_\infty) - P \int_0^{2\pi} \cot \left(\frac{u-u'}{2}\right) Im[G(u',0] \frac{du'}{2\pi}$$

$$(3.2a)$$

$$\text{Im}[G(u,0)] = \text{Im}(G_\infty) + P \int_0^{2\pi} \cot(\frac{u-u'}{2}) \, \text{Re}[G(u',0)] \, \frac{du'}{2\pi}$$

(3.2b)

where $G(W)$ is analytic in the upper-half W-plane and
$G(W) = G_\infty + O(1/|W|)$ as $|W| \to \infty$. Eq. (3.1) follows
if $G = x + iy-W$, where $W = u+iv$.

The Hilbert transforms (3.2) are also useful for
solving potential problems in the region R. If the map
function $u(e)$ is known, boundary values of a potential
ϕ on ∂R may be related to corresponding boundary values
of a potential Φ defined in the strip S in the W-plane:

$$\Phi(u) = \phi(e)$$

$$\frac{\partial \Phi}{\partial u}\Big|_{v=0} = \frac{\partial \phi}{\partial s} \Big/ \frac{du}{de}$$

(3.3)

$$\frac{\partial \Phi}{\partial v}\Big|_{v=0} = \frac{\partial \phi}{\partial n} \frac{ds}{de} \Big/ \frac{du}{de}$$

where s and n are the tangential and normal directions
to ∂R. The tangential and normal derivatives of ϕ are
the real and imaginary parts of an analytic function in S
so they are related by the Hilbert transform:

$$\frac{\partial \phi}{\partial n} \frac{ds}{de} = - \int_0^{2\pi} \cot \frac{1}{2} (u(e)-u(e')) [\frac{d\phi}{de}(e')\frac{du}{de}(e) - \frac{d\phi}{de}(e)\frac{du}{de}(e')] \frac{de'}{2\pi}$$

(3.4)

Note that in the application of (3.4) it is necessary to compute du/de with some care. We have found it best to find du/de by using the Hilbert transform of $\ln\, dz/dw$ to obtain an equation for $\ln\, du/de$.

In order to examine the crowding properties of domains bounded by breaking waves, we use (3.1) to compute the function $u(e)$ for the periodic curve

$$x(e) = e + b\, \sin e$$

$$(3.5)$$

$$y(e) = 0.4\, \sin e.$$

For $b < 1$, the curve is a single valued function of x. For $b = 1$, the curve has a vertical slope at $e = \pi$, and for $b > 1$, the function is multivalued. In Fig. 3, the curves (3.5) are plotted for $b = 1, 1.5$, and 2.0. The map function $u(e)$ must be a monotonically increasing function of e. Therefore $du/de > 0$ although it can be exponentially small due to crowding. The functions $u(e)$ and du/de are tabulated for the curves (3.5) in Table 3.1. Another measure of the crowding is given by $\ln\, (\frac{du}{de})$. In Fig. 4, $\ln(\frac{du}{de})$ is plotted for various values of b to reveal the exponetial nature of the crowding phenomenon. As b increases, the crowding rapidly becomes

severe even though the amplitude of the wave (3.5) is
quite modest. Similar crowding should be expected in
any dynamic simulation of a breaking wave.

It is also possible to formulate a set of differential
equations based on the Menikoff-Zemach approach to map
a time-dependent boundary. For parametrized boundaries
of the form $(x(e,t),y(e,t))$, the mapping function $u(e,t)$
is determined by

$$\frac{\partial u}{\partial t} = \frac{du_0}{dt} + \frac{\frac{\partial x}{\partial t}\frac{\partial x}{\partial e} + \frac{\partial y}{\partial t}\frac{\partial y}{\partial e}}{(\frac{ds}{de})^2} \quad \frac{\partial u}{\partial e} \tag{3.6}$$

$$+ \int_0^{2\pi} \cot(\frac{u(e)-u(e')}{2}) \left[\frac{\frac{\partial y}{\partial t}(e')\frac{\partial x}{\partial e}(e') - \frac{\partial x}{\partial t}(e') \frac{\partial y}{\partial e}(e')}{(\frac{ds}{de}(e'))^2} \right.$$

$$\left. - \frac{\frac{\partial y}{\partial t}(e)\frac{\partial x}{\partial e}(e) - \frac{\partial x}{\partial t}(e)\frac{\partial y}{\partial e}(e)}{(\frac{ds}{de}(e))^2} \right] (\frac{\partial u}{\partial e}(e'))^2 \frac{de'}{2\pi}$$

where $(\frac{ds}{de})^2 = (\frac{\partial x}{\partial e})^2 + (\frac{\partial y}{\partial e})^2$ and $u_0(t)$ is chosen so that
$u(0) = 0$.

Given the values of u, ϕ, x, and y at some time t
the time stepping algorithm proceeds as follows: First,
the values of $u(e)$, $x(e)$ and $y(e)$ are used to determine

the map derivative du/de. Next, the normal velocities

$\partial\phi/\partial n$ can be computed from (3.4). Once $\partial\phi/\partial s$ and

$\partial\phi/\partial n$ are known, the boundary curve $(x(e,t),y(e,t))$

can be marched to the next time step. Then, Bernoulli's

equation (1.2) gives the boundary values of ϕ at the

next step. Finally, the map Eq. (3.6) is used to march

u forward in time.

　　　We have tested the time dependent mapping equation (3.6)

on the mapping of the region bounded by a cosine curve of

increasing amplitude,

$$x(e,t) = e$$

$$(3.7)$$

$$y(e,t) = t\,\cos(e)$$

and on the regions bounded by a time dependent version of

the breaking curves (3.5),

$$x(e,t) = e + t\,\sin e$$

$$(3.8)$$

$$y(e,t) = 0.4\,\sin e.$$

　　　A fourth order Adams-Moulton predictor-corrector scheme

was used to march the map function $u(e,t)$ forward in time.

At the times tabulated in Tables 2 and 3, the mapping

function was corrected by solving (3.1). The time integration

was then restarted with the corrected values of u(e).
The maximum error for a given time is given in Tables
2 and 3 for 32, 64 and 128 points. The minimum of the
function du/de for each time is also listed to give
an indication of the crowding. The error for moderate
distortions was fairly insensitive to reductions in the
time step Δt but was reduced markedly when the number
of points was increased. In regions of severe crowding
the time step must be very small in order to ensure
accuracy for an explicit integration scheme. Too large
a time step can destroy the monotonicity of u(e).

We have also applied the integral equation (3.1)
and time-dependent evolution equation (3.6) to the
numerical simulation of Rayleigh-Taylor instability. The
initial conditions for the Rayleigh-Taylor problem are
as follows. Fluid of density 1 lies above the periodic
interface

$$y(e, t = 0) = 0.5 \cos(e)$$

$$x(e, t = 0) = e$$

and is initially at rest. Below the interface, there is
a vacuum. The resulting flow is unstable under gravitational
acceleration. The results plotted in Fig. 5 are obtained

using the integral equation (3.1). With 60 points per wavelength, we were unable to continue the calculation past a time of $t \simeq 3.5$ at which the amplitude to wavelength ratio of the spike (at $x = \pm\pi$) is about $5.4/2\pi \simeq 0.86$. The degree to which the total energy and the rate of mass flux are conserved gives a good indication of the reliability of the simulation. After a time of 3.0, there is a progressive degradation of conservation of these quantities. This deterioration is also reflected in the spike acceleration. For large t, the spike should be nearly in free fall with an acceleration of -1.0 in our units.[1] In contrast, the present simulation shows a spike acceleration which decreases (in absolute value) below 1.0 after $t = 3.0$. Hence we conclude that the results are not reliable beyond $t = 3.0$. Similarly, the time-dependent evolution equation (3.6) gives results for this problem that are reliable only until $t \simeq 3.0$.

The present conformal mapping methods give results for Rayleigh-Taylor instability that are quite good. The amplitude/wavelength ratio has increased by about a factor 10 before the 60 point calculations degrade. Menikoff and Zemach (private communication) obtain similar amplifications before their calculations break down. However, the reasons for degradation of the calculations at large time remain unclear. On the one hand, the conformal mapping methods described in this Section are capable of resolving

much more highly deformed interfaces than achieved at breakdown, even with 60 points. On the other hand, new vortex methods[1,2] have been used to calculate Rayleigh-Taylor instability with similar spatial resolution to at least twice the amplifications achieved here. It seems that our method of coupling free-surface dynamics and conformal mapping introduces numerical inaccuracies (observed as rapid oscillations of ϕ and η for $t \gtrsim 3.0$). It is possible that this deficiency may be corrected by more sophisticated conformal mapping techniques[3].

References

1. G. R. Baker, D. I. Meiron and S. A. Orszag, Phys. Fluids, $\underline{23}$, No. 8 (1980).

2. G. R. Baker, D. I. Meiron and S. A. Orszag, Vortex Simulations of Free Surface Flows, to be published (1980).

3. M. Dubiner, Ph. D. thesis, Dept. of Mathematics, M.I.T., Cambridge, MA (1980).

4. B. Fornberg, SIAM J. Sci. Stat. Comp., to be published (1980).

5. D. Gaier, "Konstruktive Methoden der Korformen Abbildung", Springer, Berlin (1964).

6. C. Gram, "Selected Numerical Methods for Linear Equations , Polynomial Equations, Partial Differential Equations,Conformal Mapping", Regnecentralen, Copenhagen (1962).

7. D. Ives, AIAA J., $\underline{14}$ (1976), 1006.

8. L. V. Kantorovich and V. I. Krylov, "Approximate Methods of Higher Analysis", Interscience, New York (1958).

9. M. S. Longuet-Higgins and E. D. Cokelet, Proc. Roy. Soc. London $\underline{A364}$ (1978), 1.

10. R. Menikoff and C. Zemach, J. Comp. Phys., to be published (1980).

11. Schwartz, L. W., J. Fluid Mech., $\underline{62}$ (1974), 553.

Table 1. Mapping functions for the 'breaking' curves (3.5).[*]

e	b = 1.0		b = 1.5		b = 2.0	
	$u(e)$	$\dfrac{du}{de}$	$u(e)$	$\dfrac{du}{de}$	$u(e)$	$\dfrac{du}{de}$
0	0.0	1.9239	0.0	2.3575	0.0	2.7670
$\dfrac{\pi}{4}$	1.5706	1.9648	1.8956	2.3030	2.2126	2.6351
$\dfrac{\pi}{2}$	2.9331	1.4326	3.4076	1.4615	3.8677	1.4772
$\dfrac{3\pi}{4}$	3.7681	7.0083×10^{-1}	4.1579	4.9413×10^{-1}	4.5352	3.0688×10^{-1}
π	4.0981	2.0146×10^{-1}	4.3291	4.7511×10^{-2}	4.6125	4.5852×10^{-3}
$\dfrac{5\pi}{4}$	4.1841	7.7401×10^{-1}	4.3387	6.4110×10^{-4}	4.6131	9.8707×10^{-7}
$\dfrac{3\pi}{2}$	4.4406	4.2459×10^{-1}	4.3440	4.0460×10^{-2}	4.6131	3.2512×10^{-5}
$\dfrac{7\pi}{4}$	5.2656	1.2741	4.7624	1.3178	4.6920	7.0508×10^{-1}

* The results were checked for 32 and 64 points and agreed to the 5 significant digits given here.

Table 2. Error in the conformal mapping of the time-dependent cosine curves (3.7)[*].

t	$\text{Min}(\frac{du}{de})$	Maximum Error (percent)		
		N = 32	N = 64	N = 128
1.0	2.23×10^{-1}	1.8×10^{-5}	3.0×10^{-10}	6.9×10^{-10}
2.0	2.54×10^{-2}	9.1×10^{-2}	2.8×10^{-5}	1.2×10^{-8}
3.0	2.19×10^{-3}	6.9	3.1×10^{-2}	7.4×10^{-7}
4.0	1.66×10^{-4}	-	1.3	3.5×10^{-4}
5.0	1.20×10^{-5}		9.9	2.1×10^{-2}

[*]   The time step is $\Delta t = 0.001$.

Table 3.   Error in the conformal mapping of the time-dependent
'breaking' curves (3.8)[*].

t	Min$(\frac{du}{de})$	Maximum Error (percent)		
		N = 32	N = 64	N = 128
.8	1.85×10^{-1}	4.5×10^{-5}	3.2×10^{-10}	1.6×10^{-10}
1.0	7.48×10^{-2}	2.0×10^{-3}	3.1×10^{-7}	3.8×10^{-10}
1.2	1.63×10^{-2}	3.9×10^{-2}	9.0×10^{-5}	6.4×10^{-10}
1.4	1.99×10^{-3}	---	4.9×10^{-3}	8.5×10^{-7}
1.6	1.02×10^{-3}	---	---	9.5×10^{-5}

* The time step is $\Delta t = 0.001$ and 48-bit mantissa arithmetic is used.

Figure Captions

Figure 1.   A schematic plot indicating the sequence of
conformal maps used to solve inviscid free
surface flow problems. Here the fluid lies
below the interface $y = \eta(x,t)$ as in the
water wave problem.

Figure 2.   A plot of the Stokes wave profile at $t = 0$
and at $t = 2\pi$. The amplitude is 80% of the
maximum Stokes wave amplitude. The FFT
time-dependent mapping equation (2.21)
is used with $N = 64$ points. The dots
indicate the numerically computed position
of the interface. The solid line is obtained
from Padé summation of the perturbation series
for Stokes waves.

Figure 3.   A plot of y vs x for the 'breaking' curves
(3.5), $x = e + b \sin e$, $y = .4 \sin e$, for
$b = 1.0,\ 1.5,\ 2.0$.

Figure 4.   A plot of $\ln\ du/de$ for the breaking curves
plotted in Fig. 3 (a) $b = 1.0$, (b) $b = 1.5$
(c) $b = 2.0$. Here the Menikoff-Zemach equation
(3.1) is solved for the conformal mapping function
$u(e)$. Observe the exponentially strong crowding
for $b > 1$.

Figure 5.   A plot of the interface $y(x,t)$ for the Rayleigh-
             Taylor instability with initial conditions
             $y(x,t = 0) = 0.5 \cos x$ $\phi(x,t) = 0$ for $t = 0.5$
             to $t = 3.5$ in steps of   0.5.   Here   60   points
             per wavelength are used.   Both the integral
             equation   (3.1)   and time-dependent equation
             (3.6)   degrade significantly in accuracy for
             $t \gtrsim 3$ at this spatial resolution.

ζ-PLANE

Z-PLANE

W-PLANE

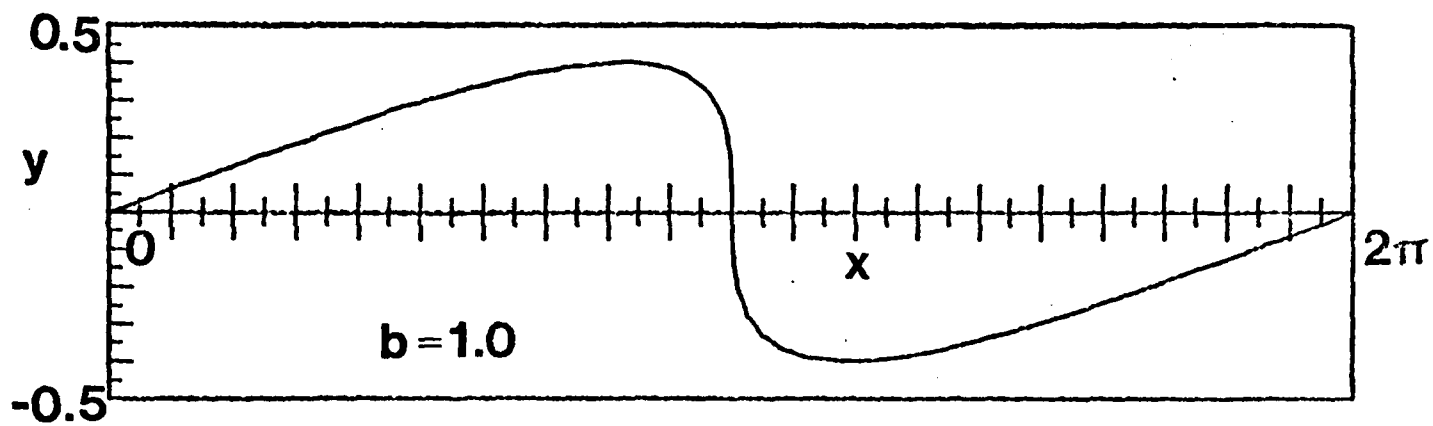$z(\zeta)$

$w=i\ln z$

$w=x+iy,$
$y=\eta(x)$

ρ

α
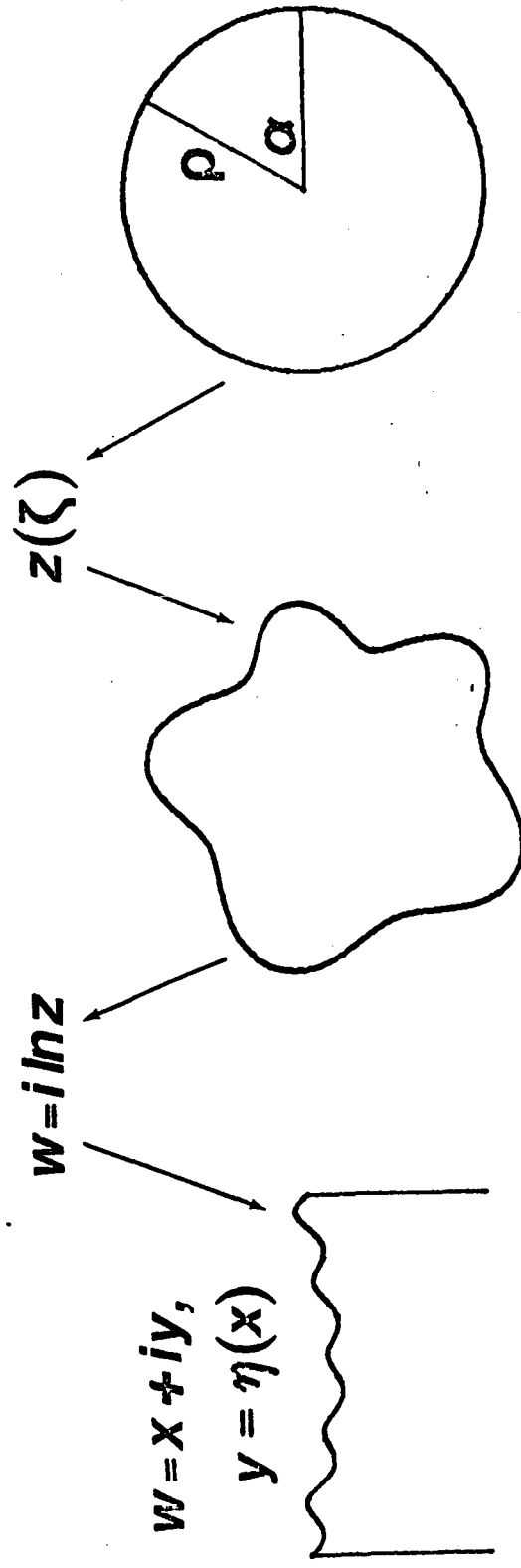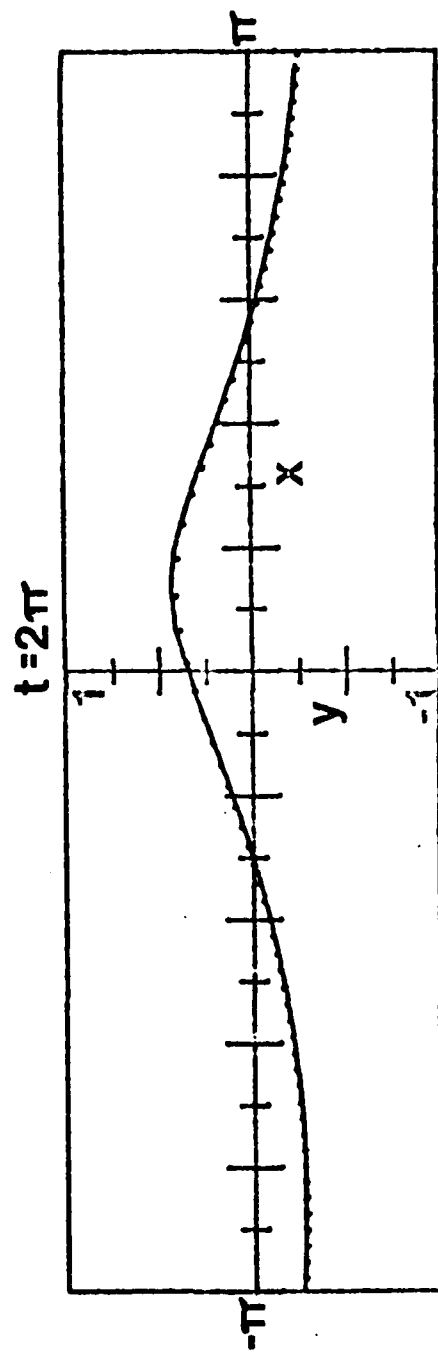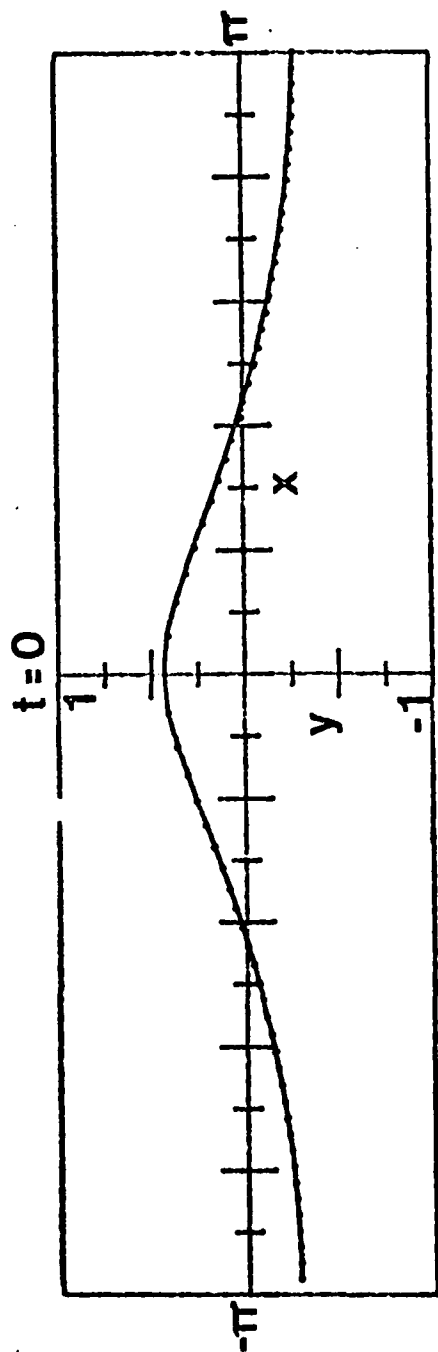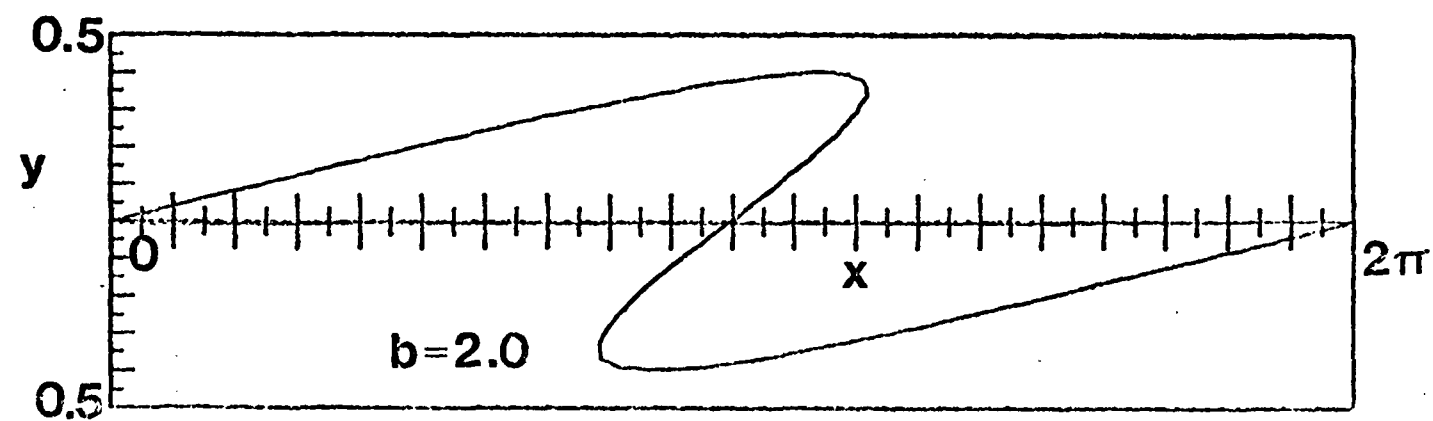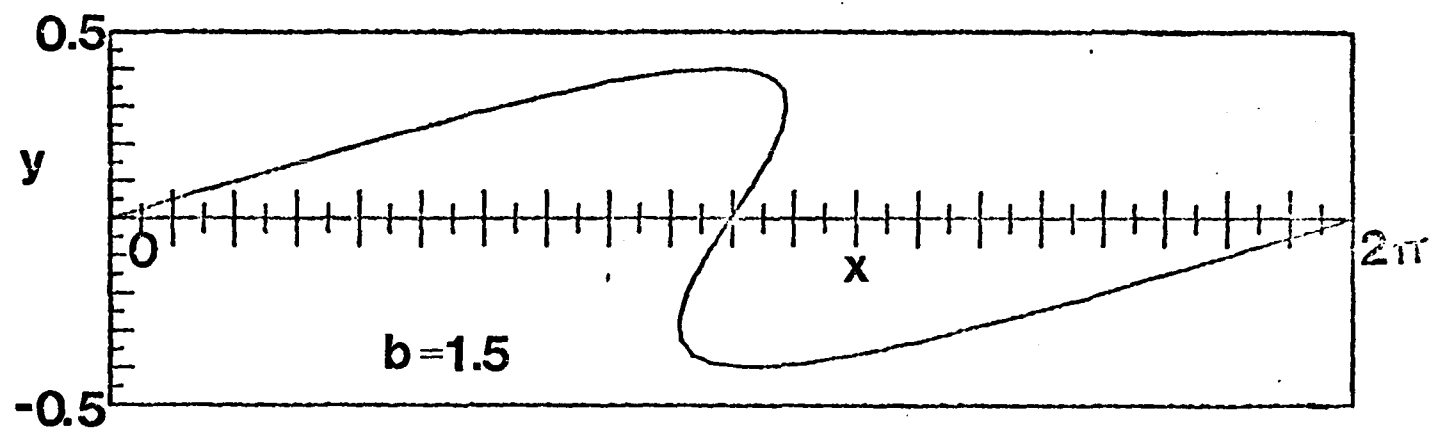
Figure 1.

Figure 2.

Figure 3.

Figure 4.

Figure 5.